Wavelet analysis of static deflections for multiple damage identification in beams

Qiaoyu Ma, Mario Solís, Pedro Galvín

Escuela Técnica Superior de Ingeniería, Universidad de Sevilla, Camino de los Descubrimientos s/n, 41092 Sevilla, Spain

Abstract

Wavelet analysis can be used in local damage detection due to its ability of revealing discontinuities induced by damage in the displacement field. This paper focuses on the application of wavelet analysis to detect and identify multiple damages using the static deflection of beams. The local damages are located by the wavelet maxima lines and their severity are evaluated from a damage index obtained from the wavelet coefficients along the corresponding maxima lines. A series of experimental tests were conducted to examine the performance of the methodology for multiple damage scenarios. The static deflections of the beam were measured by a Digital Image Correlation system. As an application, a $l1$ regularization based filter is adopted to diminish the measurement noise which is critical in the application of wavelet analysis. The paper shows the capability of using wavelet analysis for closely spaced notch-type damage detection. It also analyzes the limits of the method in estimating damage with relative small severity in the presence of severe ones.

Keywords: beams, multiple damage identification, static deflection, wavelet transform

1. Introduction

The presence of a local damage in a beam reduces its local stiffness at the damaged location, thereby altering the displacements of the beam. The difference between the intact and damaged states of the beam consists of a rapid local variation of the curvature at the damage location.

The vicinity of the damage where the curvature remains continuous but changes rapidly is known as the damage affected region. From a macro perspective, this region can be treated as a short element with a reduced stiffness or an idealized rotational spring (Friswell and Penny, 2002). In the former model, the damage leads to a discontinuity in the curvature at the boundary of the damaged element. In the latter one, the damage creates a discontinuity

Email address: msolis@us.es (Mario Solís)

in the slope of the deflection at the rotational spring. Therefore, the damage detection problem can be treated as locating discontinuities in the derivatives of the displacement field, either the static deflection or mode shapes.

Wavelet analysis is a well-known mathematical tool for detecting singularities in a signal with the advantage of being able to identify the number of irregularities along with their locations simultaneously. Therefore, it has been used for detecting local damages in beams through the displacement data, which is treated as a space signal in the wavelet analysis (Chang and Chen, 2005; Zhu and Law, 2006; Jiang et al., 2012; Solís et al., 2013; Cao et al., 2016; Ma and Solís, 2018). Damages are located at the ridges of the wavelet coefficients in the space-scale domain. Moreover, the scale parameter and the vanishing moments of the wavelet provide detailed information of the characteristic of the signal, which, in the application of damage identification, is related to the damage characteristic. The severity of damage can therefore be evaluated from the analysis of wavelet coefficients at the damage locations. The common practice is to establish a reference chart, using numerical or analytical models, which links the wavelet coefficient values and the damage severity. One direct way to build this relationship is to connect the wavelet coefficients at the damage locations of a certain scale to the damage severity (Okafor and Dutta, 2000; Umesha et al., 2009; Janeliukstis et al., 2017). Alternatively, damage indices derived from the use of wavelet coefficients across scales are proposed (Hong et al., 2002; Douka et al., 2003; Loutridis et al., 2004; Andreaus et al., 2017; Zhu et al., 2019). The major disadvantage of the proposed damage indices is that they are damage location dependent, which means the establishment of the reference chart requires the knowledge of the damage locations. For mode shape based analyses, they are also related to the mode order (Okafor and Dutta, 2000; Hong et al., 2002; Douka et al., 2003; Janeliukstis et al., 2017; Zhu et al., 2019). For static deflection based analyses, the damage indices also depend on the external load (Spanos et al., 2006; Umesha et al., 2009; Andreaus et al., 2017). (Andreaus and Casini, 2016) proposed a damage index that is independent of damage location but wavelet scale dependent.

In the application of wavelet analysis with discrete displacement data, the number of measurement points (space sampling) and measurement noise play a critical role (Quek et al., 2001; Hong et al., 2002; Gentile and Messina, 2003). The space sampling controls mainly the localization resolution and the presence of noise affects mainly the accuracy of the identification results since the wavelet coefficients are highly sensitive to local perturbations. For the successful application of wavelet analysis, sufficient displacement data are usually captured by a scanning laser vibrometer for mode shapes or a photogrammetric system for static deflections. A major difficulty is to distinguish the effect of noise from the effect of a real damage.

A useful property to be considered at this point is that the amplitudes of wavelet coefficients at the ridges due to noise do not increase with respect to the scale number as those caused by damage do. This is due to the fact that they introduce a different type of singularity. However, the upper bond of the useful scales depends on the number of measurement points between two cracks on the beam. An additional practical difficulty is that, when damages of

different severity exist throughout the structure, the damage effect caused by the less severe damage is usually masked by those induced by more severe damage (Loutridis et al., 2004; Spanos et al., 2006; Andreaus et al., 2017).

This paper presents a wavelet based approach for multiple crack identification using static deflections. First, the damage is located by using a damage locating index based on the number of local maximum values of the wavelet coefficient for all the considered scales (Zhu et al., 2019). Then, the damage severity is quantified by using a damage index based on the relationship between the wavelet coefficients at the damage positions and the scales (Ma and Solís, 2020). In contrast to the aforementioned approaches, this damage index is independent from the damage location, the load pattern and the boundary conditions.

Moreover, the paper presents experimental results of a beam with multiple damage scenarios. The displacements are measured by a Digital Image Correlation system. The use of this non-contact optical method allows a dense distribution of measurement points. In order to reduce the effect of measurement noise, a trend estimating method based on $l1$ regularization is introduced (Kim et al., 2009). It is a variation of the Hodrick-Prescott (HP) filter, in which the first norm of the curvature is used for the regularization term. As a result, the filter estimates the piecewise linear trend of a signal and it can be used to identify the first order discontinuities in the signal. The choice of the weighting parameter in the regularization term is a critical issue. In this paper, the L-curve method (Hansen, 1992) for the Tikhonov regularization problem is applied to the proposed filtering approach.

The outline of the paper is as follows. First, the theoretical basis of the damage identification approach is expounded in Section 2 and Section 3, in which the damage locating method and the quantification index are introduced. Next, a numerical example of a beam with two different boundary conditions is presented to demonstrate the performance of the proposed method in noise-free conditions (Section 4). Then, the experimental tests are described and the corresponding experimental data are used to examine the performance in real noisy situations (Section 5). At this point, the trend filtering approach is applied to diminish the measurement noise and the damage identification results are presented and analyzed. Finally, conclusions are drawn.

2. Damage induced effect in the displacement field

Let the Reference State denote the state of the beam before the occurrence of damage and the Damage State denote the state of the beam after the damage occur. If the external load remains unchanged in both the Reference State and Damage State, the change in the deflection is the result of the internal forces at the damage locations in the Reference State applied on the damaged region. The stiffness reduction at the damaged regions causes a moment redistribution along the beam. For notch type damage, assuming that there is no internal torsion created by the external loads, the deflection difference of the beam can be treated as the effect of applying a set of self-equivalent bending moments at the damage locations (Ma and Solís, 2018).

To better illustrate how the deflection difference isolates the effect of damage, let us consider a uniform beam whose length is L and has a notch at $x = a_{\in(0,L)}$ with well-established boundary conditions. The damage region is modeled by a rotational spring that connects the two undamaged parts of the beam. Its stiffness K_r is related to the damage severity. Denote the undamaged deflection of the beam by u_R and the damaged deflection by u_D under the same external load P. The equivalent state of the beam (denoted by footnote I) that can produce the deflection difference ($\Delta u = u_D - u_R$) is shown in Fig. 1, which can be described as applying the internal bending moment at the damage location at the Reference State ($M_R(a)$) as an external load on the damaged structure. The uppercase letter and the lower letter represent the external and internal bending moments, respectively. For the compatibility of the beam at the crack location, one has

$$\Delta u(a^-) = \Delta u(a^+) \tag{1}$$

$$\theta(a^-) - \theta(a^+) = \Delta\theta_I \tag{2}$$

$$m_D(a) = m_{sp} = K_r \Delta\theta_I \tag{3}$$

$$M_R(a) = m_I + m_{sp} \tag{4}$$

where θ is the slope of Δu, $\Delta\theta$ is the change of the rotation of the spring and m_{sp} is the internal moment of the spring which is also the damaged bending moment ($m_D(a)$). It can be seen that one part of the applied internal bending moment at the damage location ($M_R(a)$) is taken by the damaged cross section ($m_D(a)$) and the rest is taken by the undamaged part of the beam (m_I). In general, the shape of Δu can be represented by a piecewise cubic polynomial function. For statically determinate beams, m_I is null and the shape of Δu becomes piecewise linear.

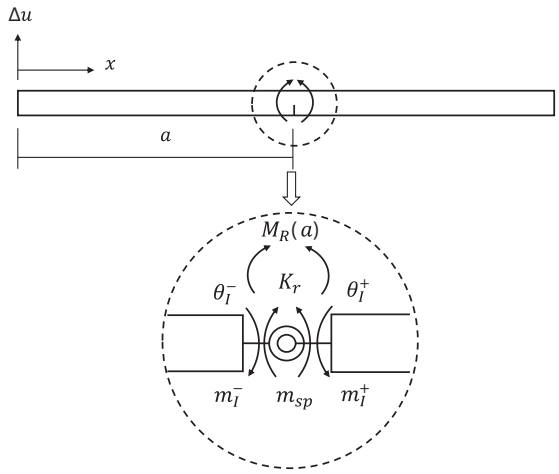

Figure 1: The equivalent state (I) of the beam that can produce the deflection difference.

3. Damage identification with wavelet analysis

A function $\psi(x) \in L^2(R)$ is said to be wavelet if it is an oscillatory function of finite length that satisfies the admissibility condition:

$$2\pi \int_{-\infty}^{+\infty} \frac{|\Psi(\omega)|}{|\omega|^2} \mathrm{d}\omega < +\infty \tag{5}$$

where $\Psi(\omega)$ is the Fourier transform of $\psi(x)$. Thus, the wavelet function is a localized signal with a zero mean and it has non-zero values within a certain interval and zero values everywhere else. This interval is known as the window size of the wavelet function and can be modified by the scale parameter s in the Continuous Wavelet Transform (CWT):

$$Wf(v,s) = \frac{1}{\sqrt{s}} \int_{-\infty}^{+\infty} f(x)\psi^* \left(\frac{x-v}{s} \right) \mathrm{d}x \tag{6}$$

where $f(x)$ is the signal, $\psi^*(x)$ is the complex conjugate of the wavelet function, v is the translation parameter and Wf is the wavelet transform of $f(x)$. The CWT measures the variation of the signal in the vicinity of v of a window size that is proportional to s through the wavelet coefficient $Wf(v,s)$. A large scale means a wide window size of the wavelet, which corresponds to a low frequency of the wavelet, whereas a small scale provides a short window size with high frequency of the wavelet. The translation parameter v controls the location of the wavelet function, thereby enabling the CWT to examine the entire signal.

A wavelet $\psi(x)$ is said to have n vanishing moments if it satisfies:

$$\int_{-\infty}^{+\infty} x^k \psi(x) \mathrm{d}x = 0, \quad k = 0, 1, 2, ..., n-1 \tag{7}$$

which means that it is orthogonal to polynomials of a degree up to $n-1$. Therefore, if a signal can be approximated by a polynomial of order $n-1$, the wavelet transform of the signal with a wavelet that has n vanishing moments is the wavelet transform of the residual between the signal and its polynomial fit.

A discontinuity in the signal can be detected by using the wavelet local maxima in the space-scale domain (the wavelet local maxima is the line that connects the local maximum values across all the scales). Let the location of the discontinuity be $v_0 \in v$, it is known (Mallat, 2009) that its wavelet coefficients across the scales satisfy:

$$|Wf(v_0, s)| \leqslant As^{\alpha+1/2} \tag{8}$$

where A is a constant and α is the Lipschitz exponent of the signal at v_0 .In this application, for which $\Delta u(x)$ is the function $f(x)$ and the discontinuity is proportional to the damaged

bending moment at the damage location $m_D(v_0)$, both sides of Eq (8) are normalized by $m_D(v_0)$:

$$NWf = \frac{|Wf(v_0, s)|}{|m_D(v_0)|} \leqslant \frac{A}{|m_D(v_0)|} s^{\alpha+1/2} \tag{9}$$

which is equivalent to:

$$\log_2(NWf) \leqslant \log_2\left(\frac{A}{|m_D(v_0)|}\right) + (\alpha + 1/2)\log_2 s \tag{10}$$

where NWf stands for the normalized wavelet coefficient. Let the straight line on the right side of Eq. (10) be the line that has the minimum slope and remains above $\log_2(NWf)$. The interception of the line with the y-axis, $\log_2(A/|m_D(v_0)|)$, is taken as the Damage Severity Index (DSI). From Eq (3), one can see that this normalization relates the DSI directly to the damage severity, thereby enabling it to be independent from the external load, the damage location and the boundary conditions.

The selection of an appropriate type of wavelet and the choice of its number of vanishing moments is essential for the effective use of wavelet analysis. A brief summary of the use of various wavelets along with the relevant researches can be found in (Rucka and Wilde, 2006). It has been found that wavelets with symmetric or nearly symmetric shape are the most useful in detecting the singularities in the displacement field. In this application, since the shape of Δu is, in general, a set of cubic functions, the wavelet from Gaussian family with four vanishing moments (Gaus4) is selected. The Gaus4 wavelet can ensure non-zero values of wavelet coefficients when the damage falls within the wavelet window only and local maximum values at the damage location.

4. Numerical illustration

A numerical case study is provided in this section to illustrate the proposed damage identification feature for notch type cracks in beams. The beams used in this simulation are modeled with 240 two-node 3D elastic beam elements (element size of 5 mm) and has a Young's modulus of 210 GPa (material of steel). The cross-section is a rectangle of a 800 mm width and a 200 mm height. Rotational springs proposed by (Ostachowicz and Krawczuk, 1991) are used for damage modeling. The rotational stiffness of the spring model is a function of the damage severity which is represented by the crack depth to cross-section height ratio (ξ). The damage scenario is set to be 4 cracks of $\xi = 10\%$, 35%, 50% and 20% at 425 mm, 525 mm, 625 mm and 775 mm, respectively, from the left end of the beam. Two boundary conditions sketched in Fig. 2 are considered, one is simply supported, denoted by Beam A, and the other is fixed fixed, denoted by Beam B. A set of concentrated loads of 120 kg each is applied at 19 distributed positions with an equal distance of 50 mm, leaving 150 mm to both ends.

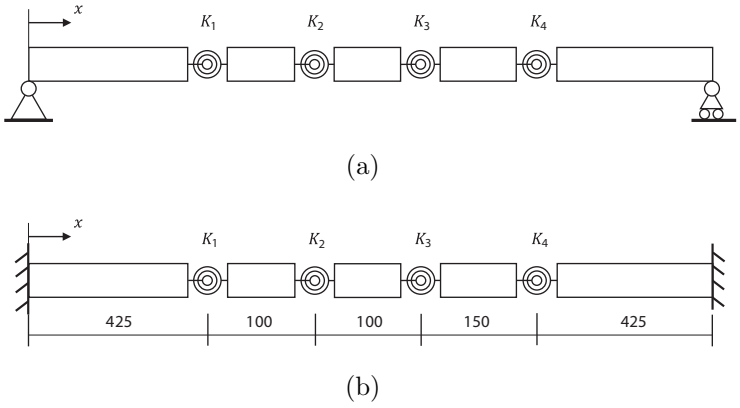

Figure 2: The scheme of the numerical models: (a) the simply supported beam (Beam A); (b) the fixed fixed beam (Beam B).

The deflections are extracted for the undamaged and damaged states at 241 nodes along the beam and the deflection differences are shown in Fig. 3(a) and (b). The wavelet coefficients of the deflection difference of the two beams are shown in Fig. 3(c) and (d) with scales from 1 to 7. Figure 3(a) and (b) show that for small damage (10% and 20%), the damage effect can be barely seen directly in the deflection difference while the discontinuities produced by 35% and 50% damage can be clearly observed. Nevertheless, all the discontinuities are clearly disclosed by the local maxima lines of the wavelet coefficients, as shown in Fig. 3(c) and (d). In this application, the wavelet maxima lines of interest connect the local minimum values of the wavelet coefficients in the space-scale domain since the values of the deflection difference are negative.

At each damage locations, the normalized wavelet coefficients and the scale parameters in the logarithmic scale are plotted in Fig. 4. The DSI is taken as the interception of the linear line which has the minimum slope and remains above the $\log_2(NWf)$ with the y-axis (see Table 1). The results show that the normalization of the wavelet coefficients leads to the same damage index for Beam A and Beam B, which verifies that the proposed DSI is independent from the influence of the boundary conditions. The authors would like to point out that the $\log_2(NWf)$ of scale 1 falls below the corresponding linear line. Hence, only higher scales would be used in processing the experimental data in Section 5. Similarly, in previous related researches (Douka et al., 2003; Loutridis et al., 2004; Zhu et al., 2019), scales higher than or equal to 2 were used.

To quantify the severity of the damage, a reference beam of the same dimension and material property is built to obtain the reference values of the DSI. A single damage is set at the mid-span of the reference beam using the same rotational spring model. Following the previously described procedure, reference values of the DSI for 10%, 20%, 35% and 50% severity are obtained (see Table 2). By comparing the DSI in Table 1 with the reference values in Table 2, the damage severity can be accurately estimated. This result verifies the independence of the DSI to the damage location and the external load. It should be noted that, in order to

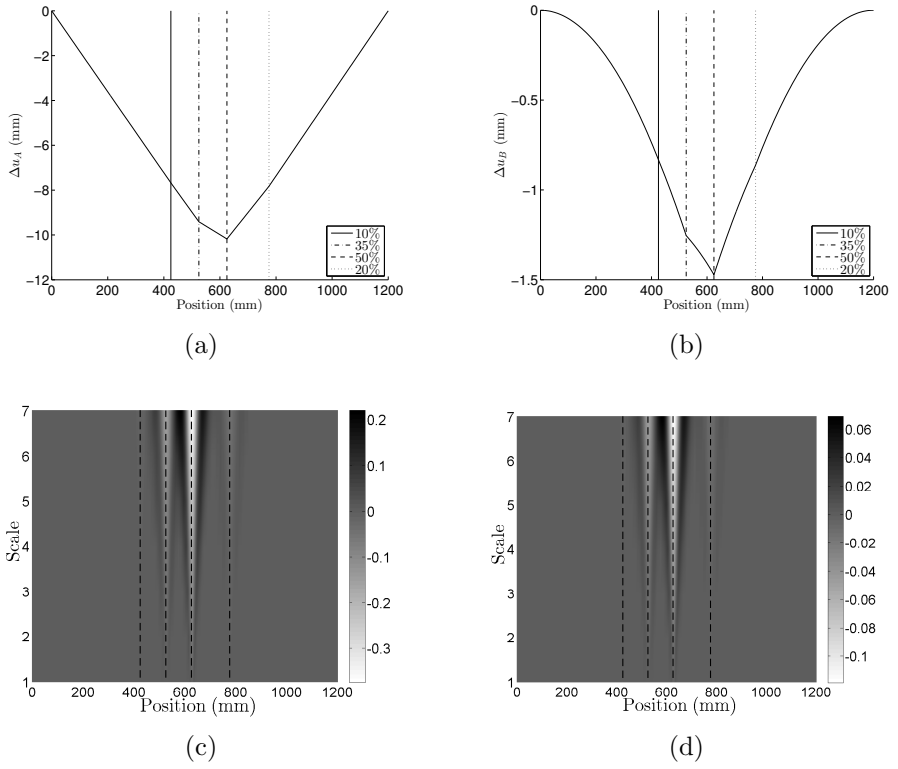

Figure 3: Numerical results: (a) the deflection difference of Beam A (Δu_A); (b) the deflection difference of Beam B (Δu_B); (c) the wavelet coefficient of Δu_A with the Gaus4 wavelet; (d) the wavelet coefficient of Δu_B with the Gaus4 wavelet. Vertical lines are superimposed at the actual damage locations.

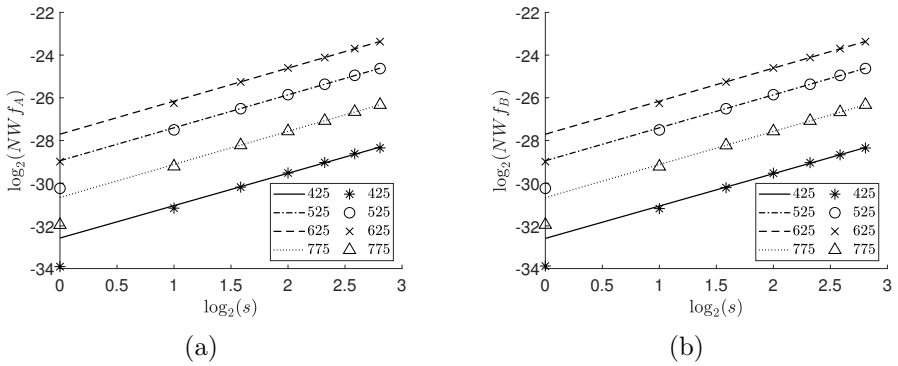

Figure 4: Normalized wavelet coefficients versus scales at damage locations in the logarithmic scale of: (a) Beam A; (b) Beam B (legend unit: mm).

match the DSI values, the wavelet function, scale parameters and measurement points for the CWT shall be identical for the reference model and the actual structure.

Although the proposed methodology exhibits an excellent performance through the numerical example, it is a practical challenge to detect relative small damage in a multiple-damage scenario in real applications with the existence of measurement noise. This issue is addressed

Table 1: The damage index of Beam A and Beam B.

Crack position (mm)	DSI	
	Beam A	Beam B
425	−32.57	−32.59
525	−28.94	−28.95
625	−27.71	−27.71
775	−30.67	−30.68

in the next section.

Table 2: The reference values of the damage index.

Damage severity $\xi(\%)$	DSI
10	−32.63
20	−30.67
35	−28.96
50	−27.71

5. Experimental tests

5.1. Test setup

To examine the performance of the proposed damage identification methodology, a series of laboratory tests of a steel beam with multiple notches were conducted. The tested steel beam has the following properties: its length is 1200mm, its width is 800mm, its height is 20mm and the Young's modulus is 210 GPa. The beam is simply supported. A mass of 120 kg was hanged at 19 equal distributed places to generate the deformation. The sum of the deflection measurements of all load positions was used. The static deflections of the beam were measured by using a Digital Image Correlation (DIC) system. The system consists of two measuring cameras of 5 megapixel resolution and uses white and black high contrasted circles as the measurement target. A number of 241 measurement points with an equal spacing of 5 mm were set on the beam. The details of the setup of the test and the measuring procedures can be found in (Ma and Solís, 2019).

First, a notch of 50% damage at 425 mm was introduced. Then, three new notches were introduced subsequently one by one at locations 775 mm, 625 mm and 525 mm, thereby reducing the minimum crack spacing from 350 mm to 100 mm. Three damage levels, 20%, 35% and 50%, were studied for each notch. The progressive sequence of increasing damage severity leads to nine damage cases defined in Table 3.

From the deflection difference of the beam in Fig. 5, one can clearly see the piecewise linear trend of Δu. The slope discontinuity caused by the 50% damage and 35% damage can be discerned in Fig. 5 by visual inspection, while the effect of the 20% damage can be barely recognized. In addition, it can be seen that as the number of damage increases and the

minimum distance among damage gets shorter, it becomes more difficult to discern the effect of each damage even if they are all of 50% damage (see Fig. 5(c), (f) and (i)).

Table 3: The definition of the experimental cases.

Case	Crack severity (%)			
	at 425 mm	at 525 mm	at 625 mm	at 775 mm
1	50	–	–	20
2	50	–	–	35
3	50	–	–	50
4	50	–	20	50
5	50	–	35	50
6	50	–	50	50
7	50	20	50	50
8	50	35	50	50
9	50	50	50	50

Although the noise level in the measurements in Fig. 5 is relatively low, the application of wavelet analysis to the raw data is not useful due to the sensitivity of wavelet analysis to small perturbations in the input signal. Figure 6 shows the wavelet coefficients of the raw data from all the damage cases using the Gaus4 wavelet. The CWT does not only result in local peaks of wavelet coefficients at the damage locations, but also at many non-damaged locations due to the effect of noise. Therefore, a denoising technique is needed to filter out false positive alarms.

5.2. Denoising

Denoising the data of the deflection difference can be understood as the problem of estimating its underlying actual trend. The choice of the trend estimating method depends on the shape of the deflection difference. In this study, due to the piecewise linearity of the deflection difference for statically determinate beams, the $l1$ Trend Filtering method is adopted (Kim et al., 2009). It is a modified HP filter, in which the regularization term values the first norm of the curvature of the estimate instead of the square of its second norm. Thus, the trend estimate is obtained by minimizing the loss function below

$$(1/2)\sum_{k=1}^{N}(\Delta u_k - \Delta u_k^{lt})^2 + \lambda \sum_{k=2}^{N-1} |\Delta u_{k-1}^{lt} - 2\Delta u_k^{lt} + \Delta u_{k+1}^{lt}| \tag{11}$$

where Δu_k is the experimental value of the deflection variation at measurement point k, Δu_k^{lt} is the corresponding estimate, N is the number of measurement points and λ is the regularization parameter which controls the trade-off between the first term which measures the size of the residual and the second term which measures the "smoothness" of the estimate or the curvature of the estimate. As the first term gets higher weight, the estimate tends to

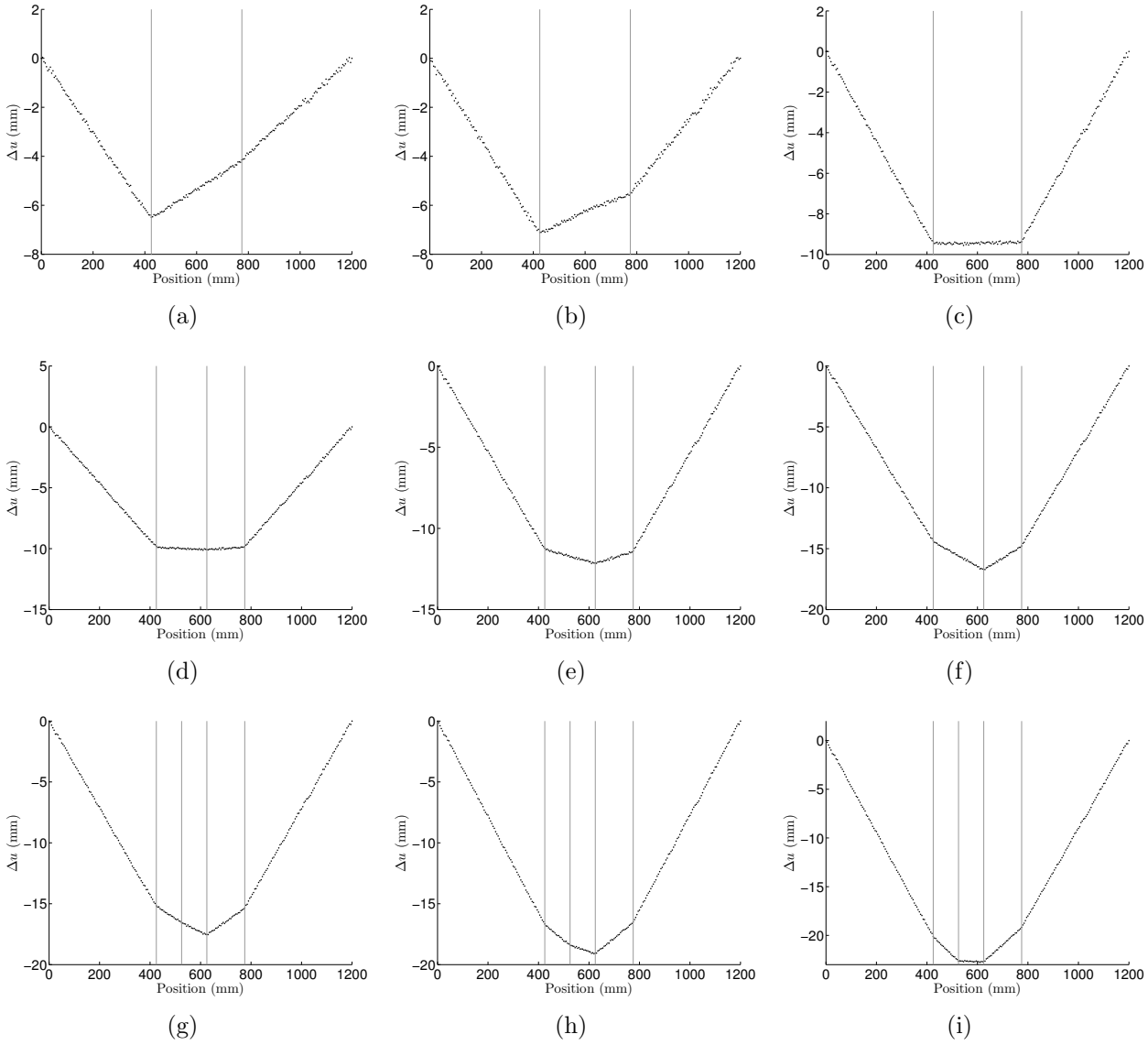

Figure 5: The deflection difference of the beam, Δu, of: (a) Case 1; (b) Case 2; (c) Case 3; (d) Case 4; (e) Case 5; (f) Case 6; (g) Case 7; (h) Case 8; (i) Case 9. Vertical lines are superimposed at the actual locations of the notches.

overfit the data. The estimate returns the original data when λ approaches 0. On the other hand, if the second term gets higher weight, the estimate tends to underfit the data. The estimate returns the linear regression fit (a straight line) of the input data when λ approaches its upper bound value (λ_{max}) which is defined as (Kim et al., 2009):

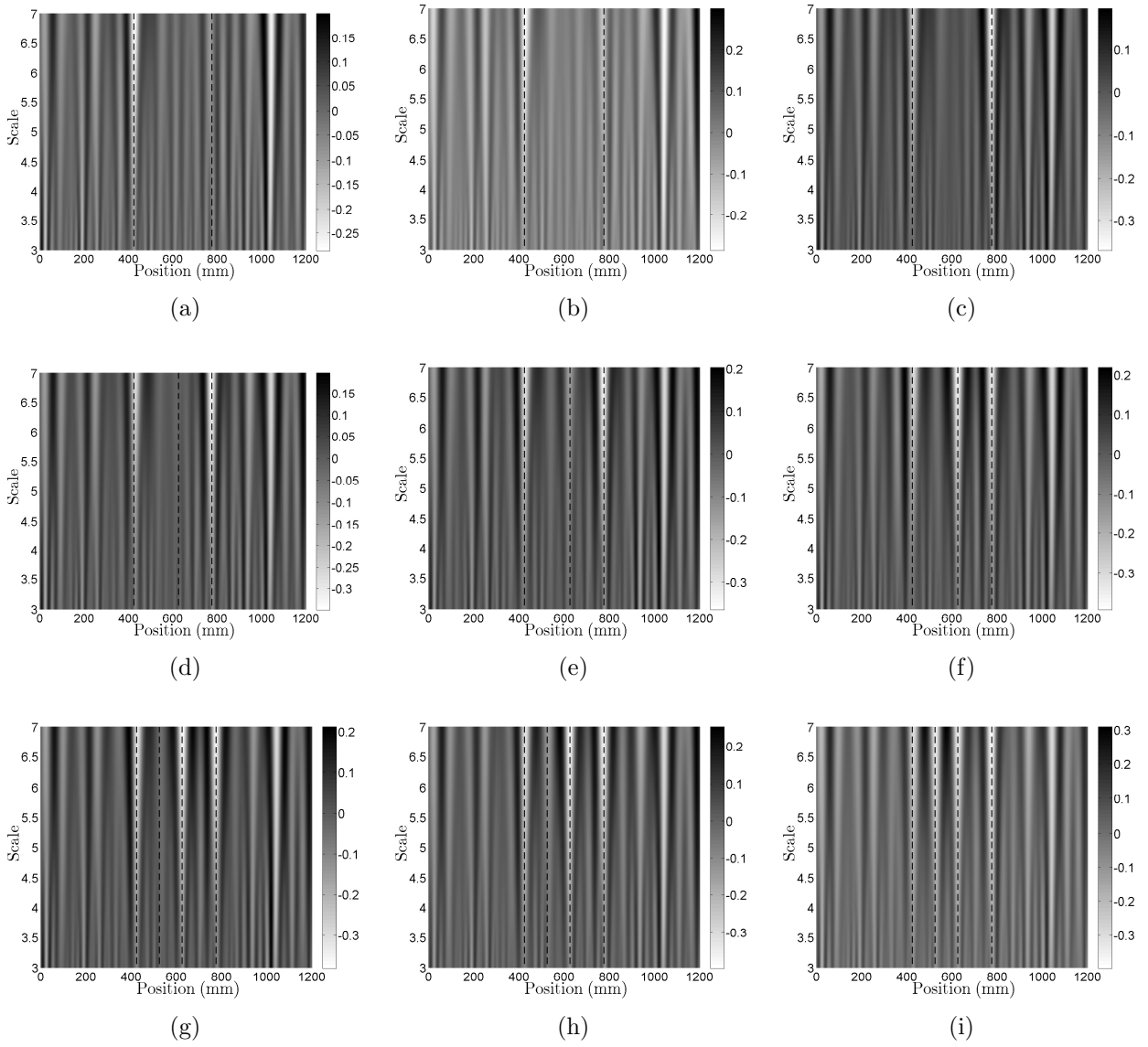

Figure 6: The wavelet coefficients of the deflection difference with the Gaus4 wavelet of: (a) Case 1; (b) Case 2; (c) Case 3; (d) Case 4; (e) Case 5; (f) Case 6; (g) Case 7; (h) Case 8; (i) Case 9. Vertical lines are superimposed at the actual locations of the notches.

.

$$\lambda_{max} = \left|\left|(DD^T)^{-1}D\Delta u\right|\right|_\infty \tag{12}$$

$$D = \begin{bmatrix} 1 & -2 & 1 & & \\ & 1 & -2 & 1 & \\ & & \ddots & \ddots & \ddots \\ & & & 1 & -2 & 1 \end{bmatrix}_{(N-2)\times N} \tag{13}$$

where $||\bullet||_p$ means the pth-norm. Equation (11) can be written in matrix form as

$$(1/2)||\Delta u - \Delta u^{lt}||_2^2 + \lambda||D\Delta u^{lt}||_1 \tag{14}$$

An appropriate value of λ should yield a good balance between the residual norm $||\Delta u - \Delta u^{lt}||_2$ and the penalty term $||D\Delta u^{lt}||_1$. This paper presents a practical criteria for selecting the value of λ. It is based on the L-curve method (Hansen, 1992), which was originally proposed for selecting the value of the regularization parameter in a Tikhonov regularization approach. In this paper, the second norm of the residual $||\Delta u - \Delta u^{lt}||_2$ is plotted versus the first norm of the curvature $||D\Delta u^{lt}||_1$ in the logarithmic scale in Fig. 7 for values of $\lambda \in [2^{-9},\ 2^{9}]$. The typical L-curve is obtained for all cases.

For small λ values , the L-curve is approximately a horizontal line and starts to bend down rapidly for a certain range of λ values. Once λ surpasses this range, the L-curve turns rapidly to be an approximate horizontal line again, on which the norm of the curvature $||D\Delta u^{lt}||_1$ becomes almost insensitive to the increase of λ. As an extension of the L-curve method, it can be stated that the values of λ at the lower "corner" of the L-curve are good candidates because in this region there is a good compromise between achieving a small curvature of the estimate $||D\Delta u^{lt}||_1$ and keeping the residual $||\Delta u - \Delta u^{lt}||_2$ reasonably small. At the region around this "corner", the sensitivity of the fitted result to the value of λ is small, which means any value from this region provides a similar estimate of the deflection difference. In this application, the selected value of λ that corresponds to the "corner" of the L-curve are shown in Fig. 7.

The output of the filter of all cases is plotted in Fig 8 for the range from 400mm to 800mm of the beam. It can be seen that, with the selected λ values, the filter provides a reasonable estimate of the trend of the deflection difference data and reduces the local effect of noise significantly.

5.3. Damage Localization

The CWT is applied to the estimates of the deflection difference to identify the potential damage locations on the beam. Following the previous discussion in the numerical example, the CWT was performed using the Gaus4 wavelet with scales $s = 3$ to 7 and the corresponding wavelet coefficients are shown in Fig. 9. By comparing the results with Fig.6, it can be clearly seen that the local peaks caused by noise are diminished and those caused by the damage effect are preserved. In order to determine the precise location of the identified damage, a Damage Locating Index (DLI) is proposed based on the work of (Zhu et al., 2019). The DLI is computed for each position as follows:

$$\mathrm{DLI}(v_i) = \sum_{j=1}^{s} \mathrm{index}_j(v_i), \quad \mathrm{index}_j(v_i) = \begin{cases} 0, & \frac{\partial Wf(v_i,s_j)}{\partial v} \neq 0; \\ 1, & \frac{\partial Wf(v_i,s_j)}{\partial v} = 0. \end{cases} \tag{15}$$

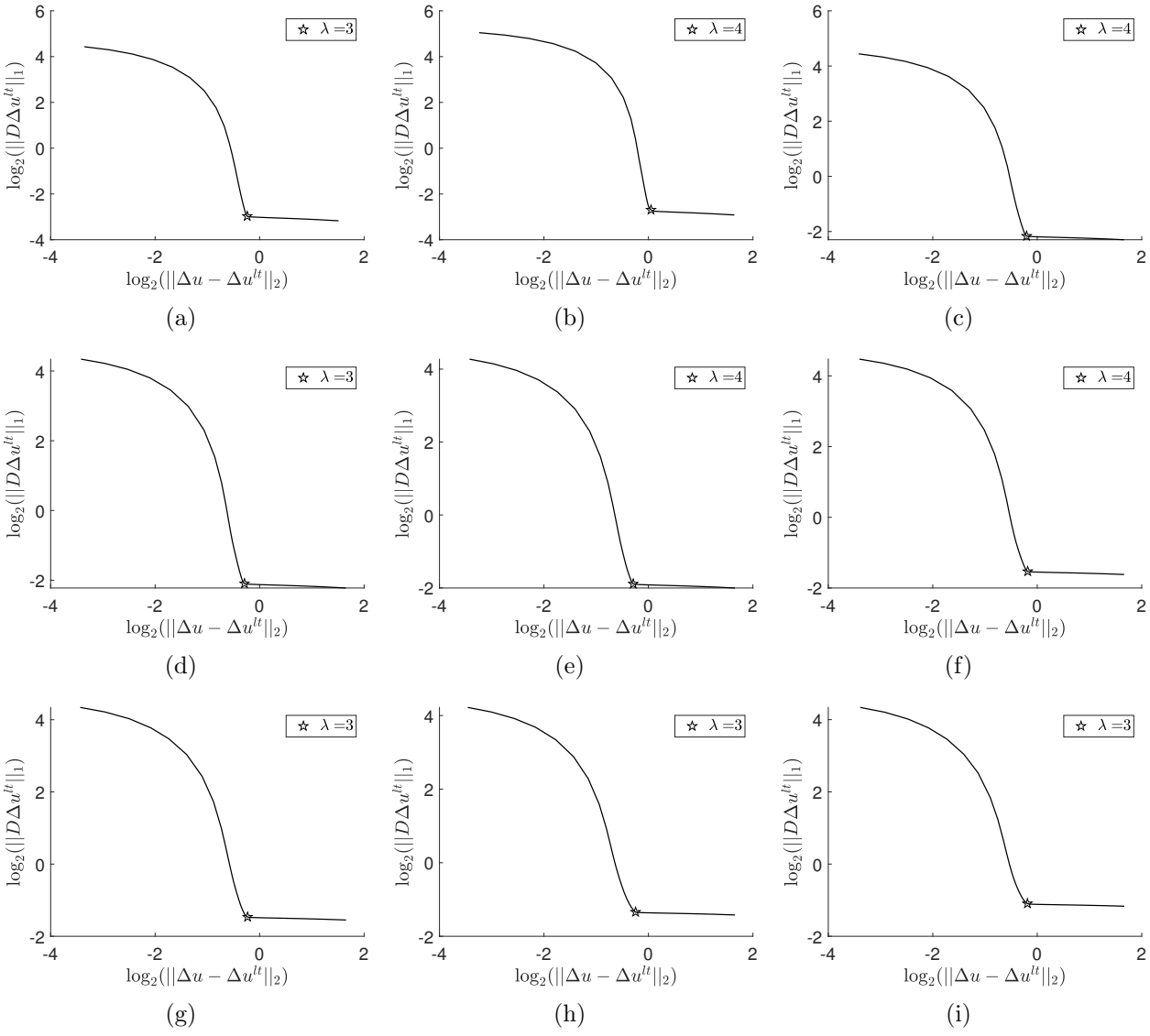

Figure 7: The L-curve of: (a) Case 1; (b) Case 2; (c) Case 3; (d) Case 4; (e) Case 5; (f) Case 6; (g) Case 7; (h) Case 8; (i) Case 9. The pentagram symbols are corresponding to the chosen λ values.

The local peaks are identified and counted for each position. In order to filter out false positives created by noise and numerical instabilities, only locations where wavelet coefficients are significant enough are considered. In this paper, only coefficients that are lower than 2% of the minimum wavelet coefficient for each scale are considered since the valid wavelet coefficients are negative. Figure 10 shows the DLI of all cases. Moreover, a potential damage location is identified when the DLI is higher than half of the number of scale parameters used in the CWT because local maximum values may shift slightly from one scale to another in real applications. In this paper, a threshold value of 3 is established as 5 values of scale were used. It successfully predicts the number and locations of the damage though one false

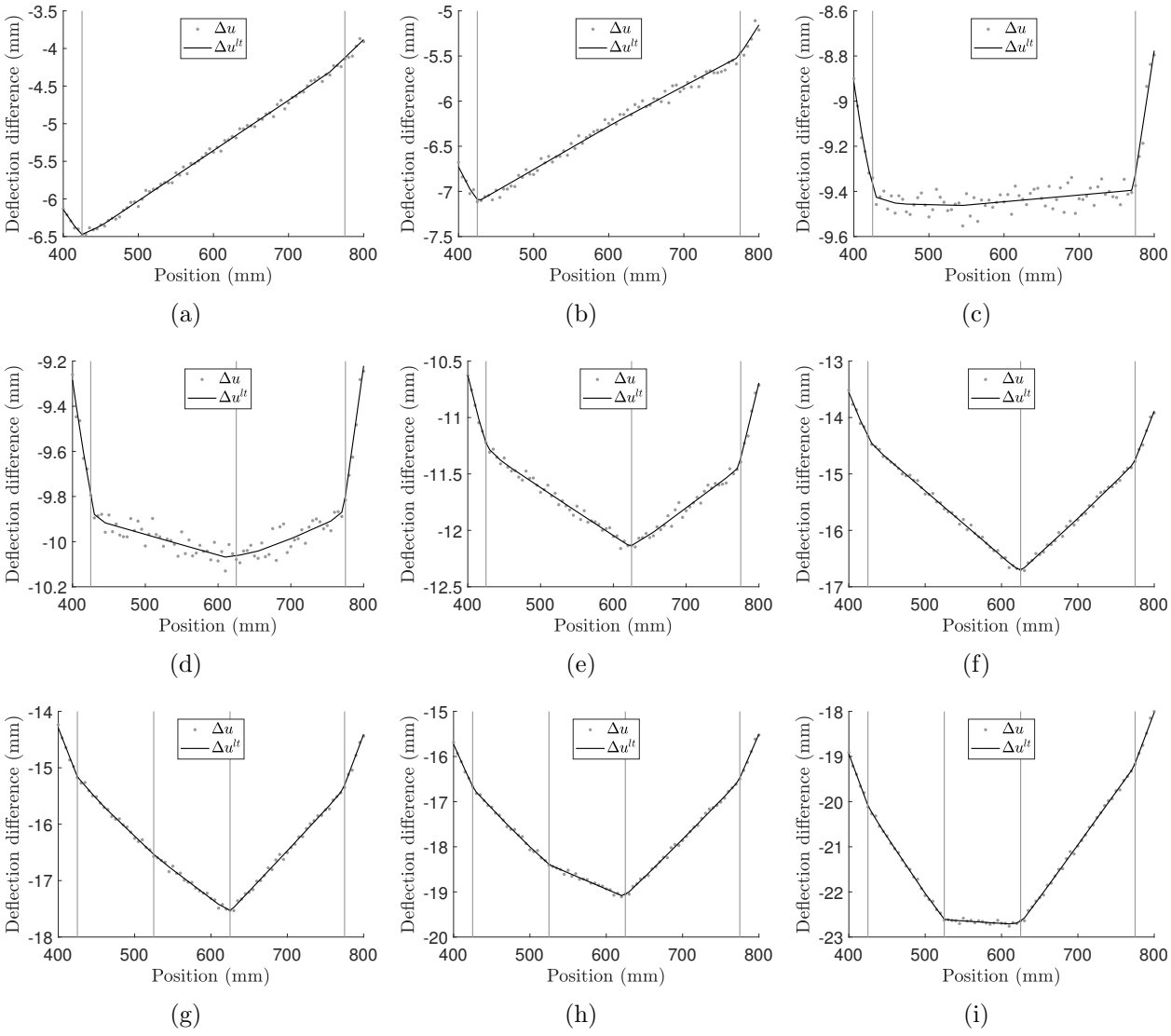

Figure 8: Original (Δu) and filtered data Δu^{lt}) between positions at 400mm and 800mm of the beam of: (a) Case 1; (b) Case 2; (c) Case 3; (d) Case 4; (e) Case 5; (f) Case 6; (g) Case 7; (h) Case 8; (i) Case 9. Vertical lines are superimposed at the actual locations of the notches.

positives are identified in Case 4, Case 5, Case 6 and Case 9. The accuracy of the damage quantification and the relevance of the false positives are discussed in the next section.

5.4. Damage Identification

Once the damage locations are identified, the DSI at each predicted damage location can be obtained by examining its wavelet coefficients across the scales, as described in Section 4. In this study, the reference values of the DSI are obtained by using a numerical 3D finite element model which has the same geometry and material properties of the experimental beam. A single crack of 1 mm width is set at location 725 mm and the boundary conditions were set

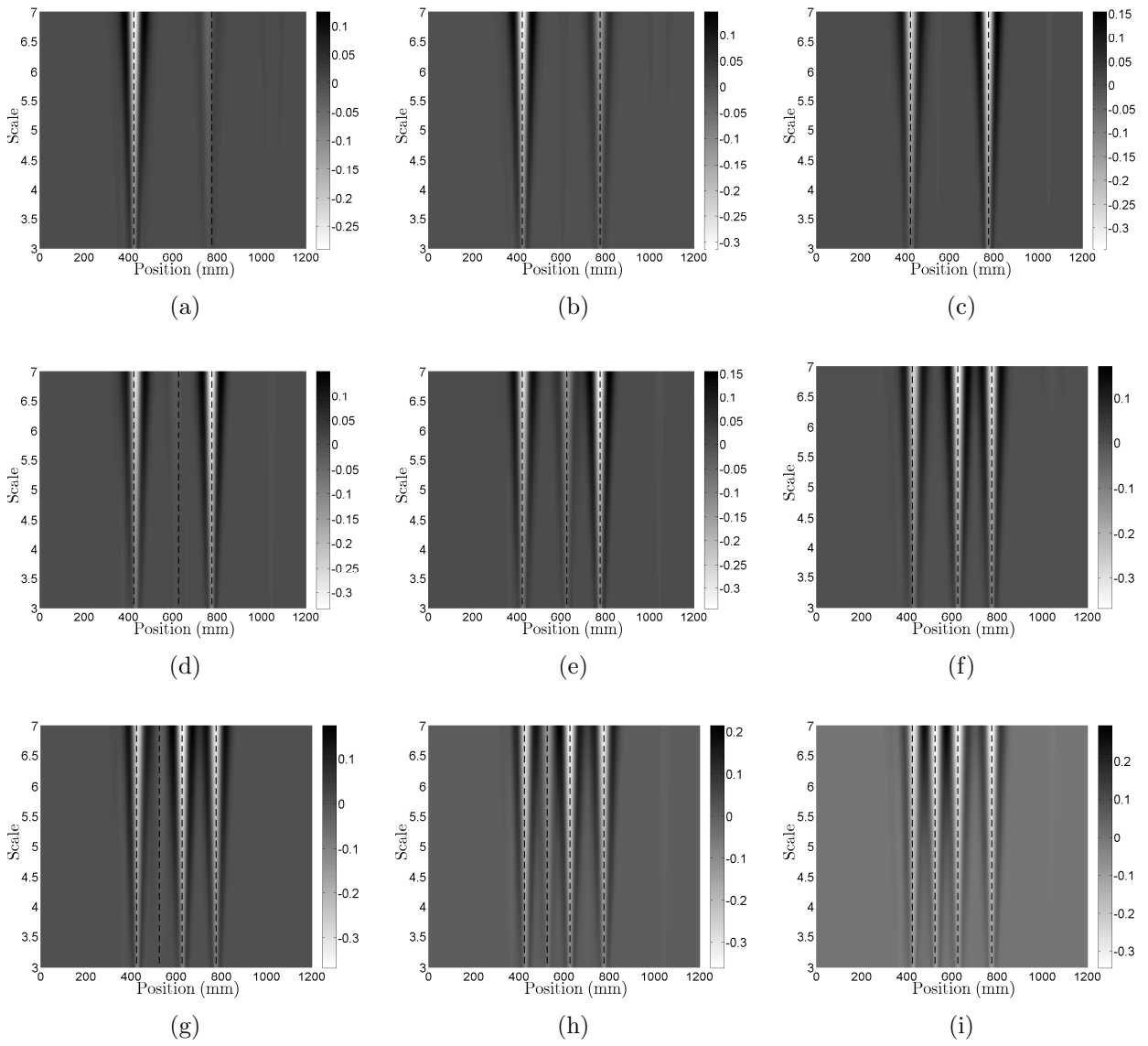

Figure 9: The wavelet coefficient of Δu^{lt} with the Gaus4 wavelet of: (a) Case 1; (b) Case 2; (c) Case 3; (d) Case 4; (e) Case 5; (f) Case 6; (g) Case 7; (h) Case 8; (i) Case 9. Vertical lines are superimposed at the actual locations of the notches.

to be simply supported. The reference values of the DSI for damage levels (ξ) from 5% to 60% are obtained with the same wavelet function and scale parameters (see Fig. 11).

The predicted damage identification results are shown in Fig. 12. It can be seen that the method identifies all the damage locations in all cases successfully. In Case 4, Case 5, Case 6 and Case 9, the method identifies a false positive alarm at location 1045 mm where no damage exist. However, the predicted severity of all the false positive alarms is less than 20% damage. In Case 3, Case 4, Case 5 and Case 6, the depth of the crack at 425 mm is

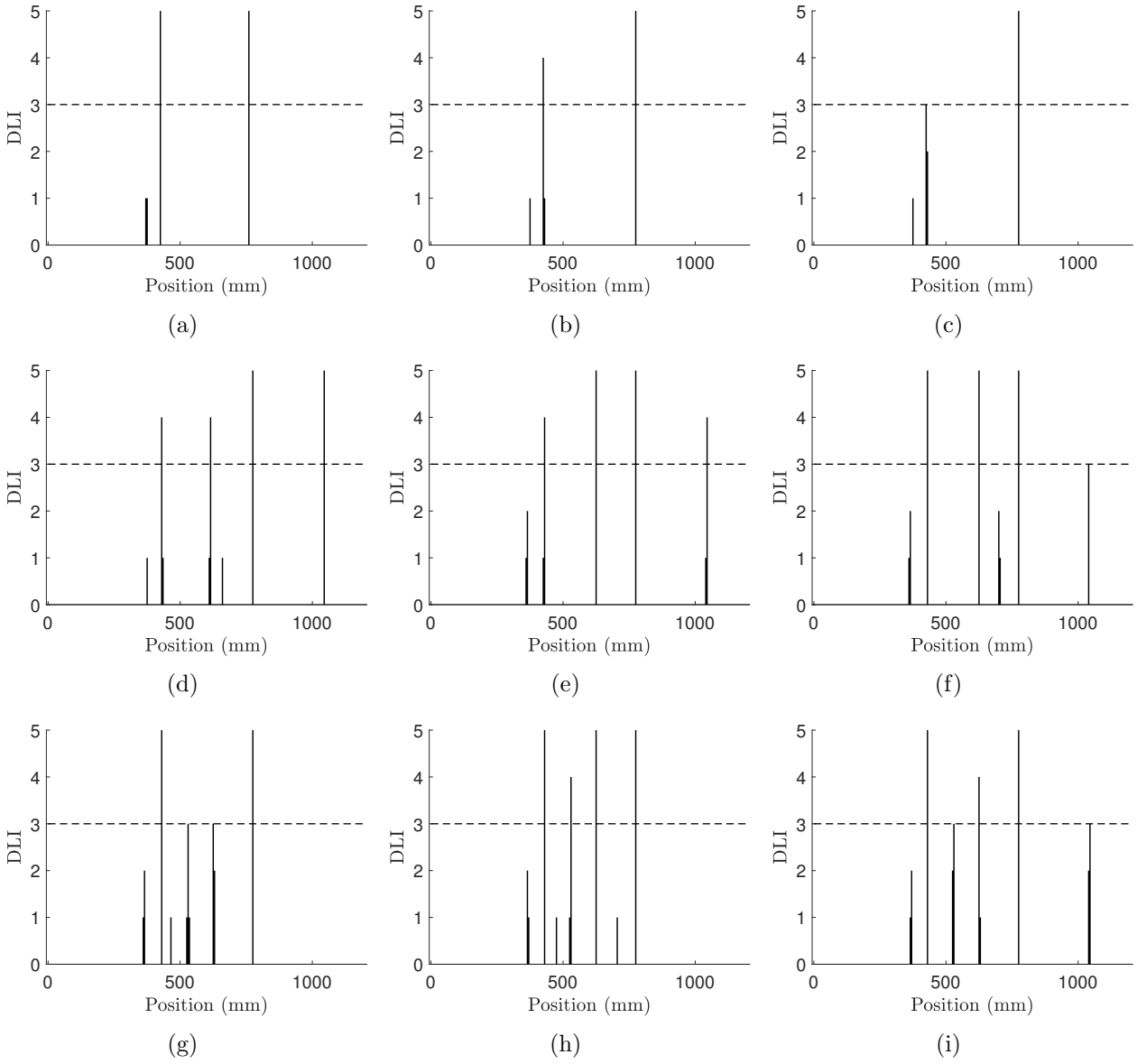

Figure 10: The Damage Locating Index of: (a) Case 1; (b) Case 2; (c) Case 3; (d) Case 4; (e) Case 5; (f) Case 6; (g) Case 7; (h) Case 8; (i) Case 9. The horizontal dashed lines mark the threshold value for determining the damage location.

underestimated. This is due to the fact that the estimate exhibits a subtle slope discontinuity close to the damage, as it can be seen in Fig. 8, which shifts the predicted damage location and reduces its predicted severity. A similar phenomenon is also observed for the damage at 625 mm in Case 9.

Regarding the identification of small damage in the presence of severe ones, the results of Case 2, Case 5 and Case 8 show that the method can accurately estimate the 35% damage. Nevertheless, for 20% damage, the results of Case 1, Case 4 and Case 7 show that the method

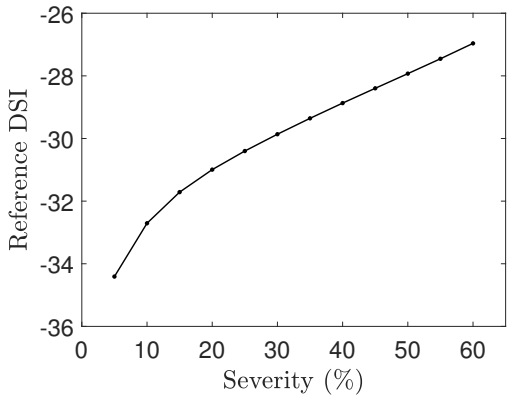

Figure 11: Reference values of the DSI.

can accurately evaluate the depth in Case 1 but the depth in both Case 4 and Case 7 is underestimated.

6. Conclusions

This paper presents a method that applies wavelet analysis for multiple notch type damage identification in beams from the static deflection difference between the pre- and post-damage states. The deflection difference isolates the damage effect which generates a sudden change at the damage locations in the displacement field. By applying wavelet analysis, the method locates the damage by determining the maxima lines of the wavelet coefficients and further evaluates the severity through a damage index which is independent from the external load, the damage location and the boundary conditions. The experimental case study shows that in order to practically apply wavelet analysis, the experimental measurement needs to be denoised. In this application, a $l1$ regularization based technique is adopted and a simple method for the selection of the regularization parameter is presented, resulting in a good estimate of the actual deflection difference.

The experimental case study also indicates that the method performs well in locating multiple damage of various damage levels with a damage spacing down to 100 mm in a beam of a 1200 length. Only one false positive low-severity damage is predicted. The method accurately identifies and quantify 35% damage in the presence of high severity damage of 50%. For a 20% damage, successful damage assessment is only observed when the crack spacing is 350 mm. When crack spacing is 200 mm or less, the method tends to underestimate the damage severity.

The proposed damage detection method can be applied for the structural health assessment of beam-like structures such as turbine-blades (Du et al., 2020), railway sleepers (Janeliukstis et al., 2019), supporting masts (Solís et al., 2010), etc. However, a static test is not usually practical for structures in service under unknown varying dynamic and static loads. In order to circumvent this limitation, the use of operational vibration modes as an input for the proposed methodology is considered by the authors as a future development.

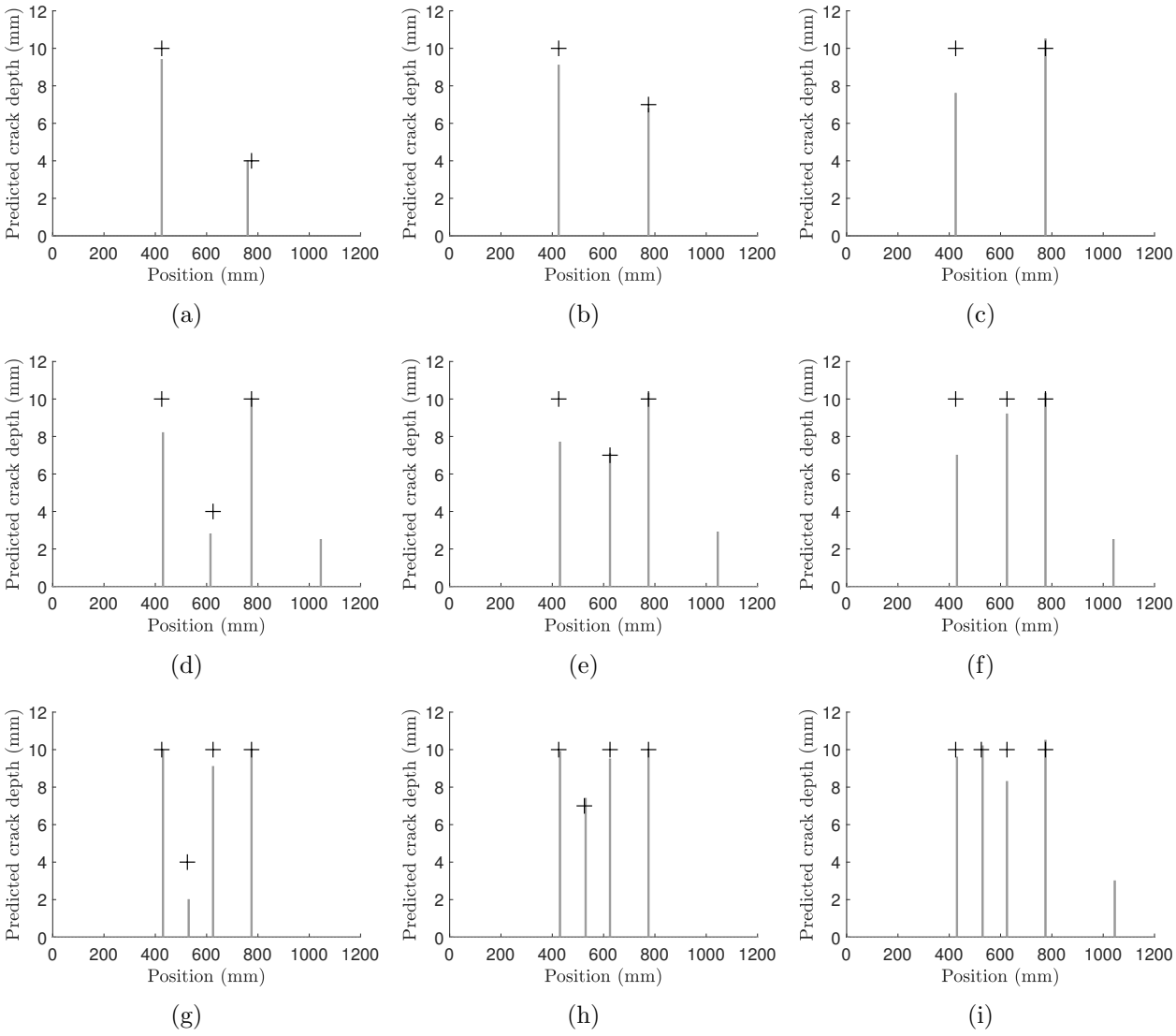

Figure 12: The estimated location and depth of the notches of: (a) Case 1; (b) Case 2; (c) Case 3; (d) Case 4; (e) Case 5; (f) Case 6; (g) Case 7; (h) Case 8; (i) Case 9. The crosses mark the actual locations and depth of the notches.

Acknowledgments

This work was supported by the Ministerio de Economía y Competitividad through research project BIA2016-75042-C2-1-R, Ministerio de Ciencia, Innovación through research project PID2019-109622RB-C21, and Consejería de Economía y Conocimiento of Junta de Andalucía (Spain) under project US-1264916. The financial support is gratefully acknowledged.

References

Andreaus, U., Baragatti, P., Casini, P., Iacoviello, D., 2017. Experimental damage evaluation of open and fatigue cracks of multi-cracked beams by using wavelet transform of static response via image analysis. Structural Control and Health Monitoring 24, 1–16.

Andreaus, U., Casini, P., 2016. Identification of multiple open and fatigue cracks in beam-like structures using wavelets on deflection signals. Continuum Mechanics and Thermodynamics 28, 361–378. doi:10.1007/s00161-015-0435-4.

Cao, M.S., Xu, W., Ren, W.X., Ostachowicz, W., Sha, G.G., Pan, L.X., 2016. A concept of complex-wavelet modal curvature for detecting multiple cracks in beams under noisy conditions. Mechanical Systems and Signal Processing 76-77, 555–575. doi:10.1016/j.ymssp.2016.01.012.

Chang, C.C., Chen, L.W., 2005. Detection of the location and size of cracks in the multiple cracked beam by spatial wavelet based approach. Mechanical Systems and Signal Processing 19, 139–155.

Douka, E., Loutridis, S., Trochidis, A., 2003. Crack identification in beams using wavelet analysis. International Journal of Solids and Structures 40, 3557–3569.

Du, Y., Zhou, S., Jing, X., Peng, Y., Wu, H., Kwok, N., 2020. Damage detection techniques for wind turbine blades: A review. Mechanical Systems and Signal Processing 141, 106445. URL: https://www.sciencedirect.com/science/article/pii/S0888327019306661, doi:10.1016/J.YMSSP.2019.106445.

Friswell, M.I., Penny, J.E.T., 2002. Crack Modeling for Structural Health Monitoring. Structural Health Monitoring: An International Journal 1, 139–148.

Gentile, A., Messina, A., 2003. On the continuous wavelet transforms applied to discrete vibrational data for detecting open cracks in damaged beams. International Journal of Solids and Structures 40, 295–315.

Hansen, P.C., 1992. Analysis of discrete ill-posed problems by means of the L-Curve. SIAM Review 34, 561–580.

Hong, J.C., Kim, Y.Y., Lee, H.C., Lee, Y.W., 2002. Damage detection using the Lipschitz exponent estimated by the wavelet transform: Applications to vibration modes of a beam. International Journal of Solids and Structures 39, 1803–1816. doi:10.1016/S0020-7683(01)00279-7.

Janeliukstis, R., Ručevskis, S., Kaewunruen, S., 2019. Mode shape curvature squares method for crack detection in railway prestressed concrete sleepers. Engineering Failure Analysis 105, 386–401. doi:10.1016/j.engfailanal.2019.07.020.

Janeliukstis, R., Rucevskis, S., Wesolowski, M., Chate, A., 2017. Multiple damage identification in beam structure based on wavelet transform. Procedia Engineering 172, 426–432.

Jiang, X., Ma, Z.J., Ren, W.X., 2012. Crack detection from the slope of the mode shape using complex continuous wavelet transform. Computer-Aided Civil and Infrastructure Engineering 27, 187–201. URL: http://doi.wiley.com/10.1111/j.1467-8667.2011.00734.x, doi:10.1111/j.1467-8667.2011.00734.x.

Kim, S.J., Koh, K., Boyd, S., Gorinevsky, D., 2009. l1Trend Filtering. SIAM Review 51, 339–360.

Loutridis, S., Douka, E., Trochidis, A., 2004. Crack identification in double-cracked beams using wavelet analysis. Journal of Sound and Vibration 277, 1025–1039.

Ma, Q., Solís, M., 2018. Damage localization and quantification in beams from slope discontinuities in static deflections. Smart Structures and Systems 22, 291–302.

Ma, Q., Solís, M., 2019. Multiple damage identification in beams from full-field digital photogrammetry. Journal of Engineering Mechanics 145, 1–12.

Ma, Q., Solís, M., 2020. Application of wavelet analysis for crack localization and quantification in beams using static deflections, in: Proceedings of the 13th International Conference on Damage Assessment of Structures, Springer, Singapore. pp. 135–149.

Mallat, S., 2009. A Wavelet tour of signal processing. 3rd ed., Academic Press, Burlington.

Okafor, A.C., Dutta, A., 2000. Structural damage detection in beams by wavelet transforms. Smart Materials and Structures 9, 906–917. doi:10.1088/0964-1726/9/6/323.

Ostachowicz, W.M., Krawczuk, M., 1991. Analysis of the effect of cracks on the natural frequencies of a cantilever beam. Journal of Sound and Vibration 150, 191–201.

Quek, S.T., Wang, Q., Zhang, L., Ong, K.H., 2001. Practical issues in the detection of damage in beams using wavelet. Smart Mater. Struct 10, 1009–1017.

Rucka, M., Wilde, K., 2006. Crack identification using wavelets on experimental static deflection profiles. Engineering Structures 28, 279–288.

Solís, M., Algaba, M., Galvín, P., 2013. Continuous wavelet analysis of mode shapes differences for damage detection. Mechanical Systems and Signal Processing 40, 645–666.

Solís, M., Romero, A., Galvín, P., 2010. Monitoring the Mechanical Behavior of the Weathervane Sculpture Mounted Atop Seville Cathedral's Giralda Tower. Structural Health Monitoring 9, 41–57. URL: http://shm.sagepub.com/content/9/1/41.abstract, doi:10.1177/1475921709340974.

Spanos, P.D., Failla, G., Santini, A., Pappatico, M., 2006. Damage detection in Euler-Bernoulli beams via spatial wavelet analysis. Structural Control and Health Monitoring 13, 472–487.

Umesha, P., Ravichandran, R., Sivasubramanian, K., 2009. Crack detection and quantification in beams using wavelets. Computer-Aided Civil and Infrastructure Engineering 24, 593–607.

Zhu, L.F., Ke, L.L., Zhu, X.Q., Xiang, Y., Wang, Y.S., 2019. Crack identification of functionally graded beams using continuous wavelet transform. Composite Structures 210, 473–485.

Zhu, X.Q., Law, S.S., 2006. Wavelet-based crack identification of bridge beam from operational deflection time history. International Journal of Solids and Structures 43, 2299–2317.